ARTICLE IN PRESS

Available online at www.sciencedirect.com

SCIENCE DIRECT®

Journal of Computational Physics xxx (2003) xxx–xxx

JOURNAL OF COMPUTATIONAL PHYSICS

www.elsevier.com/locate/jcp

First-order system least squares (FOSLS) for coupled fluid-elastic problems

J.J. Heys *, T.A. Manteuffel, S.F. McCormick, J.W. Ruge

Department of Applied Mathematics, University of Colorado at Boulder, Boulder, CO 80309, USA

Received 4 June 2003; received in revised form 29 September 2003; accepted 30 September 2003

Abstract

Mathematical models for the mechanical coupling between a moving fluid and an elastic solid are inherently nonlinear because the shape of the Eulerian fluid domain is not known a priori – it is at least partially determined by the displacement of the elastic solid. In this paper, a first-order system least squares finite element formulation is used to solve the nonlinear system of model equations using different iteration techniques, including an approach where the equations are fully coupled and two other approaches in which the equations are decoupled. The discrete linear system of equations is solved using an algebraic multigrid solver as a preconditioner for a conjugate gradient iteration. The numerical results show that the approach is optimal in the sense that computational cost is proportional to the degrees of freedom. The results also show that the choice of iteration method, from fully coupled to fully decoupled, does not significantly effect computational cost, but it does influence the error in the solution.

Keywords: Navier–Stokes; Elasticity; Coupled; Finite elements; Least-squares; Multigrid

1. Introduction

The mechanical interaction between a moving fluid and a flexible solid is an important problem in many engineering fields. The approach taken in mathematically modeling this interaction, however, strongly depends upon the properties of the fluid, fluid velocity relative to the solid, and properties of the solid. The focus here is on a moving Newtonian fluid with a Reynold's number between 0 and 500, which deforms an elastic solid with mechanical properties similar to a soft tissue. This range of properties describes many important fluid–tissue interactions in living organisms. Both the Newtonian fluid and the elastic solid may be mathematically modeled using well-known differential equations, but a number of difficulties exist for numerically approximating the solution to the coupled system of equations. First, the computational costs

* Corresponding author.
E-mail addresses: heys@colorado.edu (J.J. Heys), tmanteuf@colorado.edu (T.A. Manteuffel), stevem@colorado.edu (S.F. McCormick), jruge@colorado.edu (J.W. Ruge).

0021-9991/$ - see front matter
doi:10.1016/j.jcp.2003.09.034

for most standard techniques do not scale linearly as the problem size is increased. Second, it is often difficult, if not impossible, to accurately measure the local error in a meaningful norm. To address these limitations, a first-order system least squares (FOSLS) finite element approach is applied to the equations describing the mechanical coupling between a steady Newtonian fluid flow and an elastic solid. The goal is to develop a general approach that provides optimal scalability and a sharp error measure on model problems. The approach could then be extended to more specific applications.

The coupled fluid-elastic problem requires consideration of two different domains – the no-flow domain with the elastic solid at rest and the deformed domain with the moving fluid displacing the elastic solid. First, the no-flow domain is shown in the left half of Fig. 1, and this domain is separated into a fluid region (Ω_ξ) and a possibly multiply connected elastic region (Ω_E). The equations for the elastic solid are normally defined from the rest position of the solid, so they are based on this no flow domain. Second, the deformed fluid/solid domain is shown in the right half of Fig. 1, and the fluid region is denoted as Ω_x. The fluid equations are typically defined on the deformed domain. The interface between the two domains is Γ_x in the deformed case and Γ_ξ for the no flow domain. Mechanical coupling between the domains requires the traction to be continuous along the interface between the fluid and elastic solid regions. In the case of a non-steady problem, the velocity must also be continuous. The position of the interface and the final shape of the deformed fluid domain are not known a priori. The problem therefore requires an iterative solution technique and demonstrates nonlinear character even if the fluid equations and elastic equations are linear. A number of methods have been developed to solve this nonlinear problem, and these methods may be grouped into three categories: decoupled methods, partially coupled methods, and fully coupled methods (Fig. 2).

The most common method for solving coupled problems is a fully decoupled approach. The basic idea is to first solve the equation(s) describing the fluid on a fixed domain. The wall stress along Γ_x from the fluid solution is then used as a boundary condition when solving the elastic equation. The solution to the elastic equation includes a new position for the interface. At this point, the shape of the fluid domain has changed. Depending on the solution approach, additional equations may need to be solved to move nodes associated with the fluid discretization, or the new fluid domain may be mapped back to the original fluid domain. This process must be repeated until the boundary is no longer moving significantly and the traction is sufficiently continuous between the fluid and the solid. The primary difficulty with this approach is the potential for slow convergence and the lack of a guarantee, a priori, of convergence even if a good initial guess can be provided [1]. However, one advantage of this method is that memory requirements (and possibly CPU requirements) can be significantly reduced by decoupling the fluid, elasticity, and remeshing/remapping equations. Another advantage is that the iterations in the fully decoupled approach are frequently replaced with time steps. In this case, small time steps are often required to maintain a stable solution [2].

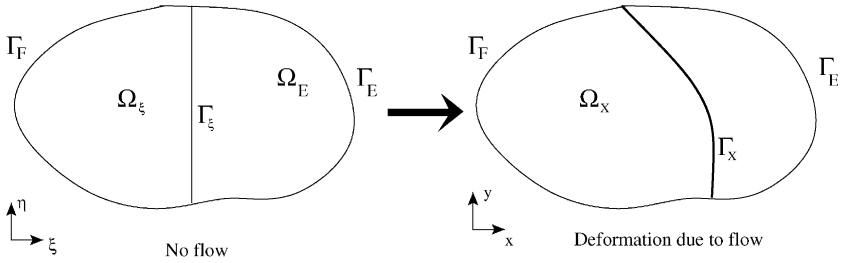

Fig. 1. The no-flow fluid (Ω_ξ) and elastic (Ω_E) domains (left) and the deformed fluid domain (Ω_x, right) for a coupled fluid-elastic system with the initial interface Γ_ξ and the deformed interface Γ_x.

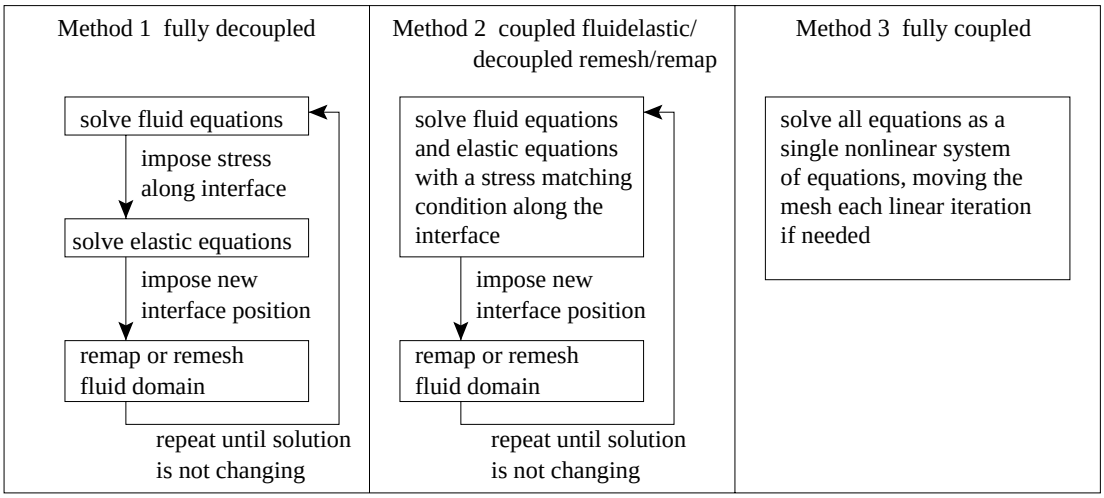

Fig. 2. Summary of the three basic methods to solve coupled fluid-elastic problems.

A simplified version of the fully decoupled approach is frequently used in modeling blood flow with the elastic domain treated as a thin shell [3,4]. The viscous shear stress is typically ignored [5], resulting in displacement only in the radial direction. An important related method is the immersed boundary method developed by Peskin [6], which uses a regular structured grid over the fluid domain, with the elastic boundary expressed in terms of a localized force distribution (Dirac delta functions) within the regular grid. The advantages of the immersed boundary method include the ability to use a straightforward finite difference approximations and the computational savings from not having to move the mesh over the fluid domain. The immersed boundary method can have problems with numerical stability if explicit time stepping is used [2], and the use of discrete delta functions prevents the method from achieving more that first-order accuracy [7].

A second method for solving coupled fluid-elastic problems is to solve the fluid and elastic equations as a coupled system of equations, but keep the moving mesh process separate. The fluid domain changes shape based on the elastic deformation, so, after completing each linearized iteration of the coupled system, the fluid mesh is moved or the fluid domain is remapped before solving the coupled system again. The first advantage to this method over the fully decoupled method is that continuity of interface tractions can be assured [8]. Under the fully decoupled approach, the interface tractions often must be transmitted between two different codes, resulting in a weakly continuous interface traction. The second advantage is that fewer iterations are typically required because the Jacobian matrix contains terms coupling the fluid and elastic domains. This helps to prevent the oscillating convergence sometimes observed with the fully decoupled method [1]. The primary disadvantages to coupling the fluid and elastic equations are the increased memory and potentially increased computational costs, although they can be somewhat reduced by modeling the elastic domain as a shell [9].

The third method is similar to the second, except the remapping or remeshing equations are solved simultaneously with the fluid and elastic equations. The result is a large system of coupled equations that potentially requires a large amount of memory to store the complex Jacobian matrix [10]. The advantages of this approach include quadratic convergence as the solution is approached and the fact that the full Jacobian contains information about the stability of converged solutions to small perturbations [10]. A final advantage is that the sensitivity of the solution to changes in parameter values is easy to predict using the full Jacobian [11].

The approximate solution found by using each of the three methods is not always the same solution. For example, if one views finding an approximate solution as minimizing the error in some norm, then it is easier to see why they can be different. In method 1, error in the fluid equations is minimized for a given domain, then error in the elasticity equations is minimized using a given traction constraint, and, finally, error in the remapping or remeshing equations is minimized for a given displacement constraint. In method 3, the sum of the error for all the equations is minimized at once, meaning that error could potentially be increased in some equations to reduce large error in other equations.

Another way to illustrate the relationship between the three methods is to view each method as solving a nonlinear problem using Newton's method. In method 1, a partial Jacobian matrix consisting of three blocks, without any coupling between the blocks, is used (the constraints are being neglected in this illustration). The three blocks can then be solved independently in a Gauss–Seidel type approach. In method 2, the incomplete Jacobian is constructed using one large block, representing the coupled fluid-elastic problem, and a separate, uncoupled block representing the remeshing or remapping problem. The full Jacobian, with coupling between the blocks, is used for method 3. The purpose of this illustration is to show that method 1 is the cheapest to solve computationally, but the inexact Jacobian may slow the convergence of Newton's method. In contrast, method 3 uses the exact Jacobian, but is the most expensive to solve computationally. The appropriate choice depends on the problem one is trying to solve. In this paper, all three methods using a FOSLS formulation are considered.

The matrix for solving the coupled fluid-elastic equations for methods 2 and 3 is neither symmetric nor positive definite if the standard Bubnov–Galerkin finite element method is used [1]. A finite element formulation that generates a symmetric positive definite matrix for all three methods is the first-order system least squares (FOSLS) approach, which is described in the next section. Previously, the FOSLS finite element formulation to solve the Stokes equations and linear elasticity equations has been shown to yield optimal discretization error estimates in the H^1 product norm and optimal algebraic convergence [12]. In addition, if elliptic grid generation (EGG) is used to map the deforming fluid domain to a reference domain, the FOSLS formulation has been shown to be H^1-elliptic, providing optimal multigrid convergence [13]. In summary, FOSLS provides optimal overall convergence properties for each of the three parts of the fluid/elastic coupled system separately. Our aim now is to test the approach on problems combining fluid, elastic, and mesh generation together.

2. Coupled fluid-elastic equations

The examples presented in the numerical results section focus on the coupling between a linear elastic solid and a Newtonian fluid. Linear elastic solids can be described by

$$-\mu_{\mathrm{E}}\Delta\mathbf{u} - (\lambda+\mu_{\mathrm{E}})\nabla\nabla\cdot\mathbf{u} = 0 \quad \text{in } \Omega_{\mathrm{E}}, \tag{1}$$

where μ_{E} and λ are Lamé constants and $\mathbf{u} = (u_1, u_2)$ is the displacement. Eq. (1) is defined on the original, undeformed domain using a Lagrangian reference frame. The coordinates for the Lagrangian reference frame are (ξ, η), and the original domain is also called the computational domain in what follows. The operators are defined as $\Delta \equiv \partial_{\xi\xi} + \partial_{\eta\eta}$ and $\nabla \equiv (\partial_\xi, \partial_\eta)^T$. Eq. (1) can be rewritten in dimensionless form by defining the following the dimensionless variables (indicated by $\hat{}$):

$$\hat{\boldsymbol{\xi}} = \frac{\boldsymbol{\xi}}{L}, \quad \hat{\mathbf{u}} = \frac{\mathbf{u}}{L},$$

where L is a characteristic length scaling. Multiplying by L/μ_{E} gives

$$-\Delta\hat{\mathbf{u}} - \left(\frac{\lambda}{\mu_{\mathrm{E}}} + 1\right)\nabla\nabla\cdot\hat{\mathbf{u}} = 0 \quad \text{in } \Omega_{\mathrm{E}}. \tag{2}$$

Newtonian fluids are modeled using the Navier–Stokes equations

$$-\rho(\mathbf{v}\cdot\nabla_{\mathbf{x}}\mathbf{v}) - \nabla_{\mathbf{x}}p + \mu_{\mathrm{F}}\Delta_{\mathbf{x}}\mathbf{v} = 0 \quad \text{in } \Omega_{\mathrm{x}}, \tag{3}$$

$$\nabla_{\mathbf{x}}\cdot\mathbf{v} = 0 \quad \text{in } \Omega_{\mathrm{x}}, \tag{4}$$

where ρ is density, p is pressure, μ_{F} is viscosity and $\mathbf{v} = (v_1, v_2)$ is velocity. Eqs. (3) and (4) are defined for an Eulerian reference frame with coordinates (x, y). The deformed fluid domain is also referred to as the physical domain. The operators are defined as $\Delta_{\mathbf{x}} \equiv \partial_{xx} + \partial_{yy}$ and $\nabla_{\mathbf{x}} \equiv (\partial_x, \partial_y)^T$. The steady-state traction matching condition between the regions is

$$\mathbf{n}\cdot\sigma_{\mathrm{E}}(\mathbf{u}) = \mathbf{n}\cdot\sigma_{\mathrm{F}}(\mathbf{v}) \quad \text{on } \Gamma_{\mathrm{x}}, \tag{5}$$

where σ_{E} and σ_{F} are the total stress tensors for the elastic solid and fluid, respectively, and $\mathbf{n}$ is the outward unit normal vector on the deformed or physical domain interface.

Eqs. (3) and (4) can be rewritten in a dimensionless form by defining the following the dimensionless variables (indicated by $\hat{}$):

$$\hat{\mathbf{x}} = \frac{\mathbf{x}}{L}, \quad \hat{\mathbf{v}} = \frac{\mathbf{v}}{\mathscr{V}},$$

$$\hat{p} = \frac{pL}{\mu_{\mathrm{F}}\mathscr{V}}, \quad Re = \frac{L\mathscr{V}\rho}{\mu_{\mathrm{F}}},$$

where L is a length scaling, $\mathscr{V}$ is a velocity scaling, and Re is the Reynold's number. Using the new variables, Eqs. (3) and (4) can be rewritten as

$$-Re\left(\hat{\mathbf{v}}\cdot\nabla_{\mathbf{x}}\hat{\mathbf{v}}\right) - \nabla_{\mathbf{x}}\hat{p} + \Delta_{\mathbf{x}}\hat{\mathbf{v}} = 0 \quad \text{in } \Omega_{\mathrm{x}}, \tag{6}$$

$$\nabla_{\mathbf{x}}\cdot\hat{\mathbf{v}} = 0 \quad \text{in } \Omega_{\mathrm{x}}. \tag{7}$$

It is important to ensure that the *dimensional* stresses are matched between the fluid and elastic solid. However, it is often desirable to match dimensionless stresses, defined as

$$\hat{\sigma}_{\mathrm{E}} = (\nabla\hat{\mathbf{u}} + (\nabla\hat{\mathbf{u}})^T) - \left(\frac{\lambda}{\mu_{\mathrm{E}}}\right)(\nabla\cdot\hat{\mathbf{u}})\delta_{ij} = \frac{\sigma_{\mathrm{E}}}{\mu_{\mathrm{E}}} \tag{8}$$

and

$$\hat{\sigma}_{\mathrm{F}} = (\nabla\hat{\mathbf{v}} + (\nabla\hat{\mathbf{v}})^T) - \hat{p}\delta_{ij} = \frac{\sigma_F L}{\mu_{\mathrm{F}}\mathscr{V}}, \tag{9}$$

where δ_{ij} is the Kronecker delta symbol. Therefore, if Eq. (5) is replaced by

$$\mathbf{n}\cdot\hat{\sigma}_{\mathrm{E}}(\mathbf{u}) = \mathbf{n}\cdot\hat{\sigma}_{\mathrm{F}}(\hat{\mathbf{v}}) \quad \text{on } \Gamma_{\mathrm{x}}, \tag{10}$$

then $\mathscr{V}$ and L must be chosen so that

$$\frac{\mu_{\mathrm{E}}}{\mu_{\mathrm{F}}} = \frac{\mathscr{V}}{L}, \tag{11}$$

thus allowing the use of dimensionless equations and dimensionless stress matching conditions. The use of a consistent length scaling, L, between the domains allows the use of a dimensionless position matching condition along the interface

$$\hat{\mathbf{x}} = \hat{\boldsymbol{\xi}} + \hat{\mathbf{u}} \quad \text{on } \Gamma_{\mathrm{x}}. \tag{12}$$

We drop $\hat{}$ in what follows since only dimensionless variables are considered.

The shape of the fluid domain is not known a priori. Therefore, elliptic grid generation (EGG) is used to map the deformed fluid region (the physical domain, Ω_{x}) back to the original computational region (Ω_{ξ}). The EGG equations are derived by requiring that the map be bijective and satisfy

$$\Delta_{\mathbf{x}}\boldsymbol{\xi} = 0 \quad \text{in } \Omega_{\mathrm{x}}, \tag{13}$$

where $\boldsymbol{\xi} = (\xi(x,y), \eta(x,y))$. Eq. (13) is defined on the unknown physical domain, Ω_{x}, but it can be inverted so that the equation is defined on the two-dimensional computational domain as follows:

$$(x_\eta^2 + y_\eta^2)x_{\xi\xi} - (x_\xi x_\eta + y_\xi y_\eta)(x_{\xi\eta} + x_{\eta\xi}) + (x_\xi^2 + y_\xi^2)x_{\eta\eta} = 0 \quad \text{in } \Omega_{\xi}, \tag{14}$$

$$(x_\eta^2 + y_\eta^2)y_{\xi\xi} - (x_\xi x_\eta + y_\xi y_\eta)(y_{\xi\eta} + y_{\eta\xi}) + (x_\xi^2 + y_\xi^2)y_{\eta\eta} = 0 \quad \text{in } \Omega_{\xi}, \tag{15}$$

where subscripts denote derivatives. The solution to the EGG equations allows Eqs. (6) and (7) to be re-written so that they are defined on the original computational domain instead of the physical domain.

Eqs. (2), (6), (7), (14) and (15) can be recast as a first-order system of equations by defining a new 2×2 matrix of variables $U = (U_{ij})$ that represent derivatives of the primary variables. Rewriting linear elasticity, Eq. (2), as a first-order system gives

$$U - \nabla\mathbf{u} = 0 \quad \text{in } \Omega_{\mathrm{E}}, \tag{16}$$

$$-(\nabla \cdot U)^T - \left(\frac{\lambda}{\mu_{\mathrm{E}}}\right)\nabla \operatorname{tr}(U) = 0 \quad \text{in } \Omega_{\mathrm{E}}, \tag{17}$$

$$\nabla \times U = 0 \quad \text{in } \Omega_{\mathrm{E}}, \tag{18}$$

where $\operatorname{tr}(U) = U_{11} + U_{22}$. For the first-order system, bold letters indicate a vector, capital letters indicate a second-order tensor, and the shape of zero is implied by the left side. Eq. (18) is added to expose divergence free errors and to establish H^1 ellipticity [14]. It is important to note that Dirichlet boundary conditions given by

$$\mathbf{u} = g \quad \text{on } \Gamma_{\mathrm{E}}, \tag{19}$$

are now supplemented with the additional tangential boundary condition of

$$\tau \cdot U = 0 \quad \text{on } \Gamma_{\mathrm{E}}, \tag{20}$$

where τ is the unit vector tangential to the interface with direction oriented clockwise. Neumann boundary conditions can be rewritten as $\mathbf{n} \cdot U = b$ where $\mathbf{n}$ is the normal vector to the boundary and b is the specified flux (cf. [14]). The Neumann and Dirichlet conditions for the fluid and EGG equations are also modified in a consistent manner.

The first-order system for the EGG equations (14) and (15) is

$$J - \nabla\mathbf{x} = 0 \quad \text{in } \Omega_{\xi}, \tag{21}$$

$$(J^{-T}J^{-1}\nabla)\cdot J = 0 \quad \text{in } \Omega_\xi, \tag{22}$$

$$\nabla \times J = 0 \quad \text{in } \Omega_\xi, \tag{23}$$

where $\mathbf{x} = (x(\xi,\eta), y(\xi,\eta))$ is the mapping from the computational domain to the physical domain (see Fig. 1) and J is the Jacobian of the mapping. Eq. (22) is nonlinear and illustrates that fluid-elastic coupled problems are always nonlinear in character, either implicitly or explicitly.

Finally, the first-order system for the Navier–Stokes Eqs. (6) and (7) is, after mapping,

$$V - \nabla \mathbf{v} = 0 \quad \text{in } \Omega_\xi, \tag{24}$$

$$(J^{-T}J^{-1}\nabla)\cdot V - (J^{-1}\nabla p_s)^T - Re(\mathbf{v}\cdot J^{-1}V) = 0 \quad \text{in } \Omega_\xi, \tag{25}$$

$$\alpha \cdot \nabla \operatorname{tr}(J^{-1}V) = 0 \quad \text{in } \Omega_\xi, \tag{26}$$

$$(J^{-1}\nabla)\cdot \mathbf{v} = 0 \quad \text{in } \Omega_\xi, \tag{27}$$

$$\nabla \times V = 0 \quad \text{in } \Omega_\xi. \tag{28}$$

By allowing $\alpha \to \infty$ (i.e., setting $V_{11} = -V_{22}$), Eq. (26) is strictly enforced which can accelerate the convergence rate of a multigrid solver by making the operator more diagonally dominant. However, by strictly enforcing Eq. (26), mass conservation in terms of the variable V is being weighted more heavily than momentum conservation. The result is less error in mass conservation and more in momentum conservation, which may or may not be desirable.

Dimensionless stress matching condition (10) between the two regions can now be rewritten in terms of first-order variables:

$$J^{-1}\bar{\mathbf{n}}\cdot\left(U + U^T + \frac{\lambda}{\mu_E}\cdot \operatorname{tr}(U)\delta_{ij}\right) - J^{-1}\bar{\mathbf{n}}\cdot(J^{-1}V + (J^{-1}V)^T - p\delta_{ij}) = 0 \quad \text{on } \Gamma_\xi, \tag{29}$$

where $\bar{\mathbf{n}}$ is the outward unit normal vector on the undeformed computational interface. The J^{-1} operator maps $\bar{\mathbf{n}}$ to $\mathbf{n}$, the vector normal to the deformed or physical interface. In many cases, it is possible to compute $\mathbf{n}$ directly, which may be desirable to prevent inaccuracies in J^{-1} from contaminating the traction matching condition.

The construction of the least-squares functional(s) from the system of first-order equations (16)–(29) depends on the method chosen to solve the coupled fluid-elastic problem (refer to Fig. 2). For the fully coupled approach, method 3, the entire system of equations is used to form a single functional:

$$\begin{aligned} G(\mathbf{u},U,\mathbf{v},V,p,\mathbf{x},J) := {} & \|U-\nabla\mathbf{u}\|^2_{0,\Omega_E} + \|-(\nabla\cdot U)^T - \left(\frac{\lambda}{\mu_E}\right)\nabla\operatorname{tr}(U)\|^2_{0,\Omega_E} + \|\nabla\times U\|^2_{0,\Omega_E} \\ & + \|J-\nabla\mathbf{x}\|^2_{0,\Omega_\xi} + \|(J^{-T}J^{-1}\nabla)\cdot J\|^2_{0,\Omega_\xi} + \|\nabla\times J\|^2_{0,\Omega_\xi} + \|V-\nabla\mathbf{v}\|^2_{0,\Omega_\xi} + \|(J^{-T}J^{-1}\nabla)\cdot V \\ & - (J^{-1}\nabla p_s)^T - Re(\mathbf{v}\cdot J^{-1}V)\|^2_{0,\Omega_\xi} + \alpha\|\nabla\operatorname{tr}(J^{-1}V)\|^2_{0,\Omega_\xi} + \|(J^{-1}\nabla)\cdot\mathbf{v}\|^2_{0,\Omega_\xi} + \|\nabla\times V\|^2_{0,\Omega_\xi} \\ & + \|J^{-1}\bar{\mathbf{n}}\cdot\left(U+U^T+\frac{\lambda}{\mu_E}\cdot\operatorname{tr}(U)\delta_{ij}\right) - J^{-1}\bar{\mathbf{n}}\cdot(J^{-1}V+(J^{-1}V)^T-p\delta_{ij})\|^2_{1/2,\Gamma_\xi}. \end{aligned} \tag{30}$$

Here, G is a single nonlinear functional that must be minimized to solve the coupled fluid-elastic problem. The boundary conditions, other than the traction matching condition, have been omitted from G because

they can be imposed on the finite element space. Alternatively, these boundary conditions can be enforced weakly in a least-squares sense by adding additional terms to the functional. We study both in our numerical tests. In G, L^2 norms are used for the domain and $H^{1/2}$ norms are used for the boundary. In the numerical implementation, L^2 norms scaled by $1/h$ are used for the weak boundary terms.

To solve the coupled problem using the fully decoupled method (method 1), three different functionals are created and minimized separately in an iterative process. The first functional, containing the fluid equations, is

$$\begin{aligned} G1(\mathbf{v}, V, p) := & \|V - \nabla\mathbf{v}\|^2_{0,\Omega_\xi} + \|(J^{-T}J^{-1}\nabla)\cdot V - (J^{-1}\nabla p_s)^T - Re(\mathbf{v}\cdot J^{-1}V)\|^2_{0,\Omega_\xi} \\ & + \alpha\|\nabla\,\mathrm{tr}(J^{-1}V)\|^2_{0,\Omega_\xi} + \|(J^{-1}\nabla)\cdot\mathbf{v}\|^2_{0,\Omega_\xi} + \|\nabla\times V\|^2_{0,\Omega_\xi}, \end{aligned} \tag{31}$$

where J is initially set to the identity matrix, and is calculated for future iterations by minimizing functional $G3$ given below. The second functional, containing the elastic equations and the stress matching condition, is

$$\begin{aligned} G2(\mathbf{u}, U) := & \|U - \nabla\mathbf{u}\|^2_{0,\Omega_E} + \|(-\nabla\cdot U)^T - \left(\frac{\lambda}{\mu_E}\right)\nabla\,\mathrm{tr}(U)\|^2_{0,\Omega_E} + \|\nabla\times U\|^2_{0,\Omega_E} \\ & + \|J^{-1}\bar{\mathbf{n}}\cdot\left(U + U^T + \frac{\lambda}{\mu_E}\cdot\mathrm{tr}(U)\delta_{ij}\right) - J^{-1}\bar{\mathbf{n}}\cdot(J^{-1}V + (J^{-1}V)^T - p\delta_{ij})\|^2_{1/2,\Gamma_\xi}, \end{aligned} \tag{32}$$

where V is given from the previous minimization of $G1$ and J is as before. Finally, using $\mathbf{u}$ from the previous minimization of $G2$, the third functional consisting of the EGG equations is

$$G3(\mathbf{x}, J) := \|J - \nabla\mathbf{x}\|^2_{0,\Omega_\xi} + \|(J^{-T}J^{-1}\nabla)\cdot J\|^2_{0,\Omega_\xi} + \|\nabla\times J\|^2_{0,\Omega_\xi}. \tag{33}$$

Note that $G2$ is linear, so $G1$ and $G3$ are the only functionals that must be minimized using multiple Newton iterations.

Method 2 is a compromise between methods 1 and 3. First, a single linear functional is created that contains both the fluid and elastic equations

$$\begin{aligned} G4(\mathbf{u}, U, \mathbf{v}, V, p) := & \|U - \nabla\mathbf{u}\|^2_{0,\Omega_E} + \|(-\nabla\cdot U)^T - \left(\frac{\lambda}{\mu_E}\right)\nabla\,\mathrm{tr}(U)\|^2_{0,\Omega_E} \\ & + \|\nabla\times U\|^2_{0,\Omega_E} + \|V - \nabla\mathbf{v}\|^2_{0,\Omega_\xi} + \|(J^{-T}J^{-1}\nabla)\cdot V - (J^{-1}\nabla p_s)^T - Re(\mathbf{v}\cdot J^{-1}V)\|^2_{0,\Omega_\xi} \\ & + \alpha\|\nabla\,\mathrm{tr}(J^{-1}V)\|^2_{0,\Omega_\xi} + \|(J^{-1}\nabla)\cdot\mathbf{v}\|^2_{0,\Omega_\xi} + \|\nabla\times V\|^2_{0,\Omega_\xi} + \|J^{-1}\bar{\mathbf{n}}\cdot\left(U + U^T + \frac{\lambda}{\mu_E}\cdot\mathrm{tr}(U)\delta_{ij}\right) \\ & - J^{-1}\bar{\mathbf{n}}\cdot(J^{-1}V + (J^{-1}V)^T - p\delta_{ij})\|^2_{1/2,\Gamma_\xi}, \end{aligned} \tag{34}$$

where J is initially the identity matrix, and is calculated for later iterations by first minimizing the functional $G3$.

By recasting the original PDEs as a first-order system, it is now necessary that the original solution be in H^2 (i.e., $(\mathbf{u}, \mathbf{v}, \mathbf{x}) \in H^2$ implying $(U, V, J) \in H^1$) in order for h-refinement of the discrete finite element problem to converge to the solution using standard H^1 finite elements. Unfortunately, the model equations often fail to exhibit such smoothness when difficulties like reentrant corners are present [15]. In such cases, the FOSLS functional cannot converge to zero as the mesh spacing, h, tends to zero. Further, the error in the solution is usually global; it is not generally restricted to the local source of the singularity. One method to handle the singularity is to add the singular functions to the finite element space [16]. Another method, used in this paper, is to unweight the functional at the source of the singularity (e.g., near the corner with the singularity). The weighting, determined by the order of the singularity, is

$$w = \left(\frac{r}{R}\right)^{\beta}, \tag{35}$$

where r is the distance from the corner, R is the size of the unweighted region (typically 10% of the domain size), and β is dictated by the strength of the singularity ($\beta = 3/2$ is used here). Corner singularities can be determined a priori from the geometry, or they can be identified using FOSLS because the element contributions to the unweighted functional will be significantly larger in the corner than elsewhere. The weighting is only used on those terms in a specific corner with a singularity. By using the unweighting, H^1 becomes dense in $H(\mathrm{div}) \cap H(\mathrm{curl})$ in the weighted functional norm, meaning that standard H^1 basis functions can be used to approximate the solution.

The equations that are used in the functional (G–$G4$) are first linearized so that the solution can be found using a Gauss–Newton approach. The value of the nonlinear functional is calculated after each Gauss–Newton step to ensure that the nonlinear functional is decreasing to a minimum. A line search in the direction of the Gauss–Newton step could be used to ensure that the nonlinear functional decreases at each step. However, for all the problems that we tested, no line search was necessary. The functional for the linearized equations is minimized over the finite element spaces by setting the Gateaux derivative to zero in the weak sense for each linearized step. A finite element basis is then chosen so that the weak form generates a matrix problem. All of the simulations presented in the results section utilized a bilinear finite element basis for all of the variables. The FOSLS formulation allows the solution spaces for the variables to be chosen independently, and there is no restrictive stability condition to satisfy. As a result, both the pressure and velocity in the Navier–Stokes equations can be approximated with a bilinear basis. The finite element solution of the linearized functional is an "energy-orthogonal" projection of the exact solution of the weak equations onto the finite element space. Moreover, the finite element solution is the minimizer of the linearized functional over the finite element space. The individual components of the functional have been shown to be locally H^1 equivalent under certain assumptions; see [13] for EGG, [12] for elasticity, and [17] for Navier–Stokes (assuming that the solution is not at a bifurcation point). Ellipticity has not been proven for the functionals that combine the components together (G and $G3$). The functionals G–$G4$ measure the first derivative of the error in the primary variables (i.e., velocity, pressure, and displacement), unlike the error in the L_2 sense. Therefore, error characterized by "wiggles" in the solution, which may be small and hidden in the L^2 norm, are large and thus controllable in the functional norm.

Before describing the method for solving the linear system of algebraic equations, it is important to summarize the many levels of iteration that take place in solving these coupled problems:

- The outermost level consists of cycling between the equations (e.g., fluid, then solid, then mapping equations for the fully decoupled method) or a Newton iteration for the fully coupled method. In the FOSLS formulation, this outer process consists of iterating between functionals $G1$, $G2$, and G3, or linearizing the functional G and iterating. This process is referred to as "outer iterations".
- If method 1 or 2 is used (functionals $G1$–$G4$), the Navier–Stokes equations (functional $G1$) and the EGG equations (functional $G3$) are nonlinear and must be solved by linearizing the functionals and then iterating. These iterations are referred to as the "inner iterations".
- Finally, the inner most processes are the AMG/CG iterations, to be described in the following paragraph, that are used to solve the linear system.

The linear system is solved using an algebraic multigrid (AMG) preconditioner [18,19] for a conjugate gradient (CG) iteration. Under this AMG/CG method, a single V-cycle is used to calculate a preconditioner for a single CG iteration. Most of the computational cost is associated with the V-cycle. A full multigrid (FMG) type approach is used to reduce the number of outer iterations performed on the fine grid. This is accomplished by first performing multiple iterations on the coarser grids, where approximate solutions are found with relatively fewer calculations. The coarser grid solutions are then used as approximations for the successively finer grids. Codd [20] showed previously for a FOSLS formulation of the EGG equations that,

under certain conditions, only one linearization step is required on each grid to achieve accuracy comparable to the finest-level discretization. (Grid refinement is achieved by halving the mesh size, h, resulting in four times the number of unknowns.) A similar approach is used to obtain the results presented here. First, four outer iterations are used on the coarsest grid to find a solution there. Then, a *single* outer iteration and, if using methods 1 or 2, a *single* inner iteration, is performed on each successively finer grid until the desired finest-level is obtained. A second outer iteration can be performed as a check to ensure that the first was sufficient on the finest grid. The result is a technique in which most of the inner and outer iterations are performed on coarse grids, where the computational costs are significantly lower.

3. Simple coupled domain

The domain for the first test problem is shown in Fig. 3. For the fluid inlet and outlet, the dimensionless pressure is set to 1 and 0, respectively, and the velocity in the tangential direction, v_2, is set to 0. No-slip conditions for the fluid are imposed along the bottom and interface boundaries. The elastic solid boundary conditions consist of zero displacement in both directions along the upper boundary, zero displacement in the normal direction along the sides, and zero stress on the normal face in the tangential direction (i.e., no shear stress). For the EGG equations, the nodes along the fluid inlet and outlet are allowed to slide in the tangential direction, and orthogonality of the grid lines is strictly enforced on the inlet and outlet. All other EGG boundary conditions are homogeneous Dirichlet conditions, with the exception of the interface, where the displacement of the nodes is set to the displacement of the elastic material, Eq. (12). The test problem shown in Fig. 3 was solved using all three methods described in the introduction. For all three methods, $Re = 100$, $\lambda/\mu_E = 9.3$, and $\alpha \equiv \infty$ (i.e., $V_{11} = -V_{22}$) were used. Convergence, for all three methods, was defined as the functional changing by less that 1% between outer iterations.

Fig. 4 shows the solution to the coupled system of equations using the fully coupled approach (method 3). With this method, the full functional, $G(\mathbf{u}, U, \mathbf{v}, V, p, \mathbf{x}, J)$, is minimized to find the solution. As Fig. 4 shows, the pressure is highest at the inlet and lowest at the outlet. The higher inlet pressure causes the elastic material to be displaced upward near the inlet. Even though $Re = 100$, the flow is relatively parabolic and only slightly downward. Fig. 5 is the solution to the same coupled problem, only here we used the fully decoupled method (method 1). No single functional is minimized in this case. Instead, a series of minimization problems are solved until the iterations converge to a solution. The solutions for both methods are very similar, and as the mesh size approaches zero, the solutions become identical. The difference in practice is primarily a consequence of the fact that method 1 tends to shift error from the fluid equations to the mapping equations. Therefore, if the fully coupled approach is used, proper scaling between the functional

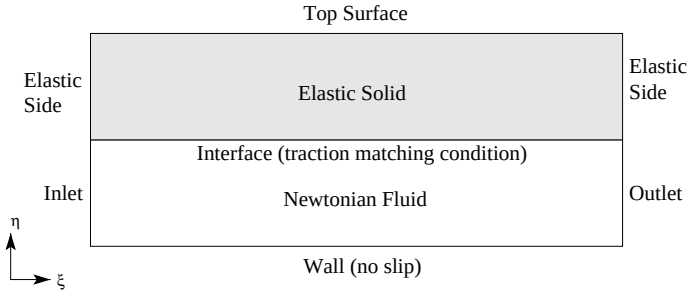

Fig. 3. Simple coupled domain. A coupled problem with a linear elastic solid above a Newtonian fluid. Both domains have an aspect ratio of 5:1. The dimensionless pressure at the inlet is set to 1 and 0 at the outlet.

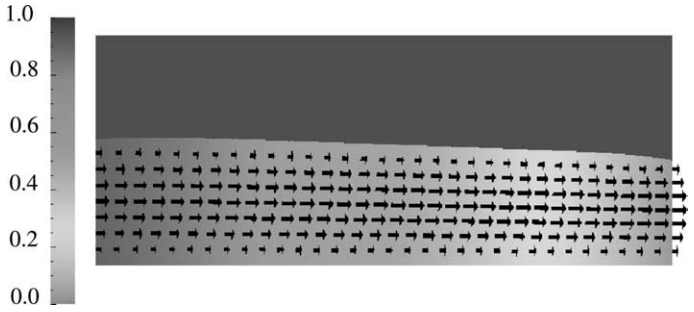

Fig. 4. Solution of the simple rectangular domain problem using the fully coupled method (method 3). The higher pressure at the inlet displaces the solid upward.

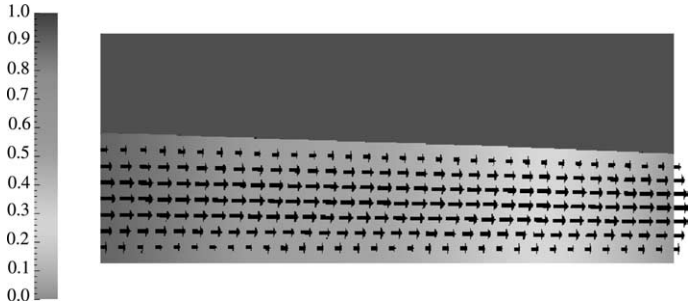

Fig. 5. A second solution for the simple rectangular domain using the fully decoupled method (method 1). The solution is almost identical to the solution from the fully coupled method.

terms associated with Navier–Stokes and the functional terms associated with EGG is important. For this problem, no scaling was required or used because the equations, in non-dimensional form, are correctly scaled. The shifting of error phenomena for the fully coupled method also explains why the solutions are identical when the mesh spacing is zero: there is no error to shift.

The numerical performance of the FOSLS finite element formulation with an AMG/CG solver on the simple coupled domain is summarized in Fig. 6. For the decoupled methods (method 1 and 2), the functionals of the individual pieces are added together in an attempt to measure the total error in the solution. Because the problem is properly non-dimensionalized, the value of the functional, which represents the error in the solution on a given grid, is independent of the solution method chosen. The small differences that are present likely result from small differences in the accuracy of the solution to the discrete problem. In other words, the discrete problem is never solved exactly using AMG/CG, only approximately so that the solution is within about 10% of discretization error. The cost of solving the problem on a given mesh is highest for the fully coupled method. This is somewhat surprising since AMG/CG is an optimal solver (i.e., the computational cost is proportional to the number of unknowns). However, there is some additional computational overhead associated with the larger matrix that results in slightly increased cost. Further, the differences between the methods appear to diminish as the mesh is refined. It is not known if the fully coupled method tends to become the most efficient computational method with very fine grids, but this is considered unlikely because it always requires the largest matrix.

The performance of the AMG/CG solver can be measured by the convergence factor for the V-cycle/CG iterations, defined as the relative decrease in the residual per $V(1,1)$-cycle/CG iteration. The computational

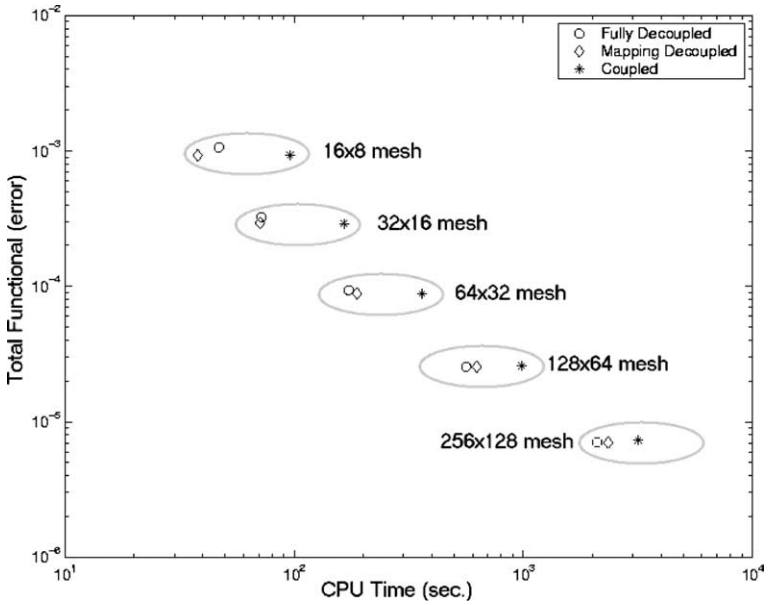

Fig. 6. The total functional (error) for different different CPU times on the first test problem. Each of the three methods is shown, and the solution was obtained on meshes of 16×8, 32×16, 64×32, 128×64, and 256×128.

Table 1
Convergence rates for the AMG/CG solver for the simple coupled domain

	Navier–Stokes	Elasticity	EGG
Decoupled	0.60	0.85	0.20
Mapping decoupled	0.87		0.20
Coupled	0.82		

The three different rates for the decoupled problem correspond to the rate for the Navier–Stokes equations, elasticity equations, and the EGG equations.

costs of a single $V(1,1)$-cycle is equal to the cost of two to three Gauss–Seidel iterations on the finest grid. In other words, if the convergence factor is 0.50, the cost of reducing the residual by 50% is of the same order as a couple of Gauss–Seidel iterations. The convergence rate given is from the finest grid used, but since there was no significant change between the two finest grids, the convergence rate is not expected to grow as the mesh size goes to zero. Table 1 summarizes the convergence rates for each of the three methods. The highest convergence rates correspond to the equations associated with the elastic domain. The lowest rates are associated with the EGG equations, which is not surprising since they are closely related to Laplace's equation. Clearly, improvements to the solver performance on the elasticity equations would be the most valuable.

3.1. Nonlinear material laws

One of the major limitations of the equations utilized in this paper is the assumption of a completely linear elastic material, which is only appropriate for a select group of materials undergoing small strains and small displacements. It is important to note, however, that nonlinear elasticity equations would not

significantly increase the computational costs because the additional iterations could mostly, if not entirely, be performed on the coarse grid. Further, while nonlinear materials are the subject of a future paper, simulations have been performed on the simple rectangular domain using a neo-Hookean material law [21]. For this problem, the computational costs increased by less than 2% for the fully coupled method, and the value of the functional also change by less than 10%.

4. L-shaped domain

Almost all problems that involve a mechanical coupling between a fluid and solid also require a more complex domain than that used in the previous section. Here we look at a mechanically coupled system on an L-shaped domain (Fig. 7). The inner part of the "L" is the elastic solid, which is fixed along its outer edge. The inner edge of the solid is the interface between the fluid and solid, and it has a traction matching boundary condition. The ends of the solid domain are fixed in the normal direction but are allowed to slide in the tangential direction through the use of a boundary condition that enforces no tangential stress. For the fluid domain, the inlet pressure is set to 1.0 and the outlet pressure is set to zero. The tangential velocity at the inlet and outlet is also set to zero. The outer edges of the "L" domain have symmetry type boundary conditions, which consist of zero normal velocity and zero tangential stress. Because of the symmetry conditions, this L-shaped domain can be considered to be one quarter of a cross-shaped domain that has two inlets and two outlets (see Fig. 8).

The discrete solution for the L-shaped domain from a 40×20 mesh, duplicated so that is shows the full symmetric flow for the cross-shaped domain, is shown in Fig. 8. This simulation used $\alpha \equiv \infty$ (i.e., $V_{11} = -V_{22}$), $Re = 20$, and, for the solid, $\lambda/\mu_E = 6.0$. The pressure is highest at the inlet, so the walls near there are compressed and thinner. The shear from the fluid displaces some of the elastic solid from the corner region toward the outlet, and the solid near the outlet is not significantly displaced because the stress is close to zero. The flow is parabolic at the inlet and outlet, and it remains laminar due to the relatively low Reynold's number. If the Reynold's number is set too high, the flow will not be laminar and the assumption of symmetry will be violated.

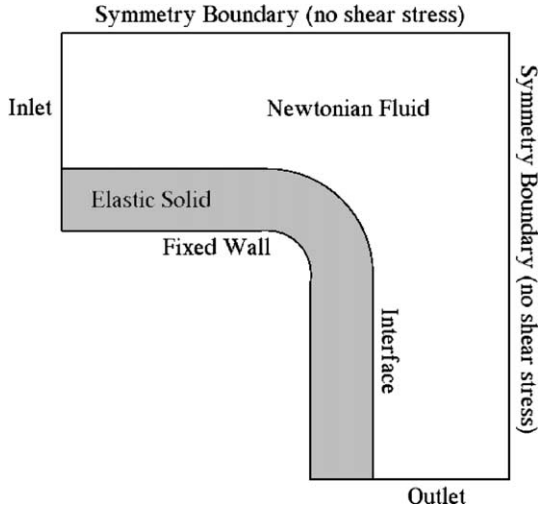

Fig. 7. The L-shaped domain for a coupled problem with a linear elastic solid wall and Newtonian fluid. The upper boundary and the right boundary have symmetry boundary conditions so that the domain represents the lower quarter of the cross-shaped domain. The outer edge of the elastic solid is assumed to be fixed.

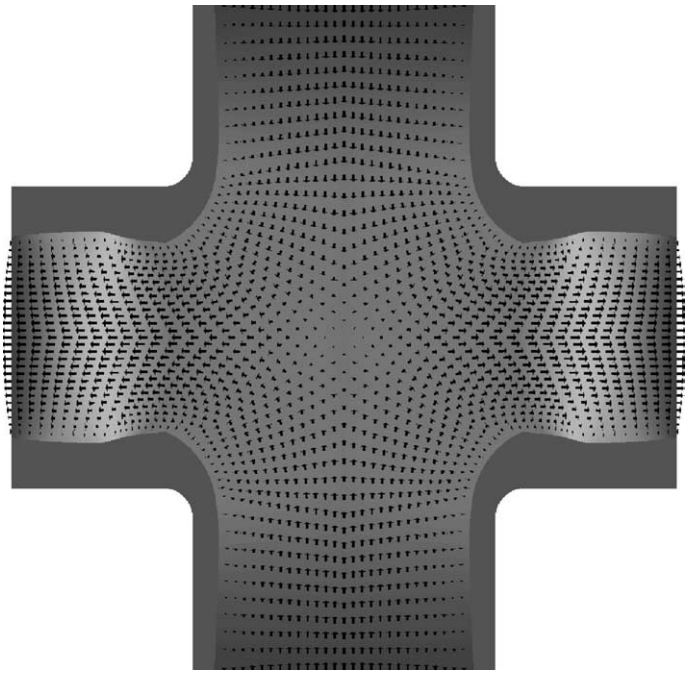

Fig. 8. The cross-shaped connection with inflow on the top and bottom and outflow on the sides. The simulation was run using the mapping decoupled method and was only run on a quarter of the symmetric domain, but was duplicated to show the full connection.

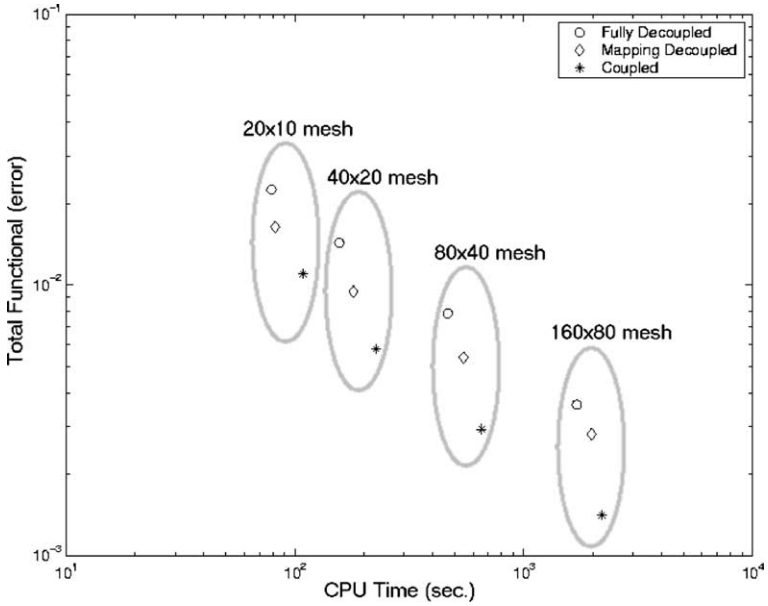

Fig. 9. The total functional (error) for different different CPU times on the L-shaped domain problem. Each of the three solution methods is shown, and the simulation was run on meshes of 20×10, 40×20, 80×40, and 160×80.

Table 2
Convergence rates for the AMG/CG solver for the L-shaped domain

	Navier–Stokes	Elasticity	EGG
Decoupled	0.60	0.90	0.55
Mapping decoupled	0.90		0.55
Coupled	0.85		

The three different rates for the decoupled problem correspond to the rate for the Navier–Stokes equations, elasticity equations, and the EGG equations.

The numerical performance of each of the three possible solution methods using a FOSLS formulation is summarized in Fig. 9. As with the previous test problem, the computational cost is highest for the fully coupled method, but, again, the difference in cost between the methods decreases as the problem size is increased. The differences in error for a given mesh were significant between the different methods. The sum of the functionals for the three parts (Navier–Stokes, elasticity, and EGG) of the fully decoupled method had the largest error. The fully coupled method, however, is guaranteed to find the minimum error for the full system of equations, and that is reflected in the results. Unfortunately, with the fully coupled method, error can be effectively transferred from one set of equations (usually Navier–Stokes) to another set of equations (usually EGG). So the mapping is slightly distorted to reduce the error in the mapped Navier–Stokes equations. This phenomena can be reduced through the use of scaling, but this was not used here for pedagogical reasons. Finally, the differences in error between the methods vanishes as the mesh size tends to zero if all singularities are properly unweighted, and, in this case, the error for all three methods appear to be vanishing at similar rates.

The performance of the AMG/CG solver on the L-shaped domain problem is consistent with the results on the simple rectangular domain as shown in Table 2. The primary difference is the increase in the convergence factor for the EGG equations. The mapping in this case is more distorted and the EGG equations are less easily solved on non-convex domains.

5. Conclusions

Mechanically coupled systems consisting of a flowing fluid and a linear elastic solid have been solved on two different domains. The first was a simple rectangular domain with the elastic material above the fluid. The second was L-shaped with the inner edge of the "L" being curved. In both cases, the FOSLS finite element formulation of the model equations achieved the two desired objectives:

- optimality in the sense that the computational costs were proportional to the number of fine grid degrees of freedom, and
- sharp error measure provided by the functional.

The first objective was realized, in part, because most of the outer iterations were performed inexpensively on a coarse grid. This fact suggests that the transition to problems with more nonlinearity, including nonlinear elasticity, should not dramatically increase computational cost.

Acknowledgements

This work was sponsored by the National Institute of Health under Grant No. 1-R01-EY12291-01, the Department of Energy under Grant Nos. DE-FG03-94ER25217 and DE-FC02-01ER25479, and the National Science Foundation under VIGRE Grant No. DMS-9810751.

References

[1] M. Heil, Stokes flow in an elastic tube – a large-displacement fluid structure interaction problem, Int. J. Numer. Methods Fluids 28 (1998) 243–265.
[2] C. Tu, C. Peskin, Stability and instability in the computation of flows with moving immersed boundaries: a comparison of three methods, SIAM J. Sci. Statist. Comput. 13 (6) (1992) 1361–1376.
[3] K. Perktold, G. Rappitsch, Mathematical modeling of local arterial flow and vessel mechanics, in: J. Crolet, R. Ohayon (Eds.), Computational Methods for Fluid–Structure Interaction, Pitman Research Notes in Mathematics Series, vol. 306, Longman Scientific and Technical, Wiley, New York, 1994, pp. 230–245.
[4] D. Tang, D. Anderson, S. Biz, D. Ku, Steady viscous flow in constricted elastic tubes subjected to a uniform external pressure, Int. J. Numer. Methods Eng. 41 (1998) 1391–1415.
[5] K. Perktold, G. Rappitsch, Computer simulation of local blood flow and vessel mechanics in a compliant carotid artery bifurcation model, J. Biomech. 28 (7) (1995) 845–856.
[6] C. Peskin, Numerical analysis of blood flow in the heart, J. Comput. Phys. 25 (1977) 220–252.
[7] M.-C. Lai, C. Peskin, An immersed boundary method with formal second-order accuracy and reduced numerical viscosity, J. Comput. Phys. 160 (2000) 705–719.
[8] O. Ghattas, X. Li, A variational finite element method for stationary nonlinear fluid–solid interaction, J. Comput. Phys. 121 (1995) 347–356.
[9] L. Formaggia, J. Gerbeau, F. Nobile, A. Quarteroni, On the coupling of 3D and 1D Navier–Stokes equations for flow problems in compliant vessels, Comput. Methods Appl. Mech. Eng. 191 (6–7) (2001) 561–582.
[10] M. Rast, Simultaneous solution of the Navier–Stokes and elastic membrane equations by a finite element method, Int. J. Numer. Methods Fluids 19 (1994) 1115–1135.
[11] J. Heys, V. Barocas, M. Taravella, Modeling passive mechanical interaction between aqueous humor and iris, J. Biomech. Eng. 123 (6) (2001) 540–547.
[12] Z. Cai, T. Manteuffel, S. McCormick, First-order system least squares for the stokes equations, with application to linear elasticity, SIAM J. Numer. Anal. 34 (5) (1997) 1727–1741.
[13] A. Codd, T. Manteuffel, S. McCormick, J.W. Ruge, Multilevel first-order system least squares for elliptic grid generation, SIAM J. Numer. Anal., to appear.
[14] Z. Cai, T.A. Mantueffel, S.F. McCormick, First-order system least squares for second-order partial differential equations: Part ii, SIAM J. Numer. Anal. 34 (2) (1997) 425–545.
[15] P. Grisvard, Elliptic Problems in Nonsmooth Domains, Pitman, Boston, 1985.
[16] G. Strang, G.J. Fix, An Analysis of the Finite Element Method, Prentice-Hall, Englewood Cliffs, NJ, 1973.
[17] P. Bochev, Z. Cai, T. Manteuffel, S. McCormick, Analysis of velocity–flux first-order system least-squares principles for the Navier–Stokes equations: part 1, SIAM J. Numer. Anal. 35 (1998) 990–1009.
[18] A. Brandt, Multi-level adaptive solutions to boundary value problems, Math. Comput. 31 (1977) 333–390.
[19] J. Ruge, K. Stüben, Algebraic multigrid, in: S.F. McCormick (Ed.), Multigrid Methods, Frontiers in Applied Mathematics, vol. 3, SIAM, Philadelphia, PA, 1987, pp. 73–130.
[20] A. Codd, T. Manteuffel, S. McCormick, Multilevel first-order system least squares for nonlinear partial differential equations, SIAM J. Numer. Anal., to appear.
[21] R. Batra, Linear constitutive relations in isotropic finite elasticity, J. Elasticity 51 (1998) 243–245.